

# A Study of Connections Between Solar Flares and Subsurface Flow Fields of Active Regions

Yu Gao · Junwei Zhao · Hongqi Zhang

Received: 16 November 2012 / Accepted: 6 March 2013 / Published online: 4 April 2013  
© Springer Science+Business Media Dordrecht 2013

**Abstract** We investigate the connections between the occurrence of major solar flares and subsurface dynamic properties of active regions. For this analysis, we select five active regions that produced a total of 11 flares with peak X-ray flux intensity higher than M5.0. The subsurface velocity fields are obtained from time–distance helioseismology analysis using SDO/HMI (*Solar Dynamics Observatory/Helioseismic and Magnetic Imager*) Doppler observations, and the X-ray flux intensity is taken from GOES (*Geostationary Operational Environmental Satellites*). It is found that among the eight amplitude bumps in the evolutionary curves of subsurface kinetic helicity, five (62.5%) of them had a flare stronger than M5.0 occurring within 8 hours, either before or after the bumps. Another subsurface parameter is the Normalized Helicity Gradient Variance (NHGV), reflecting kinetic helicity spread in different depth layers; it also shows bumps near the occurrence of these solar flares. Although there is no one-to-one correspondence between the flare and the subsurface properties, these observational phenomena are worth further studies to better understand the flares' subsurface roots, and to investigate whether the subsurface properties can be used for major flare forecasts.

**Keywords** Sun: photosphere · Sun: helicity · Sun: flare

---

Solar Origins of Space Weather and Space Climate

Guest Editors: I. González Hernández, R. Komm, and A. Pevtsov

---

Y. Gao (✉) · H. Zhang

National Astronomical Observatories of China, Chinese Academy of Sciences, Beijing, P.R. China

e-mail: [gy@bao.ac.cn](mailto:gy@bao.ac.cn)

H. Zhang

e-mail: [h Zhang@bao.ac.cn](mailto:h Zhang@bao.ac.cn)

J. Zhao

W.W. Hansen Experimental Physics Laboratory, Stanford University, Stanford, CA 94305-4085, USA

e-mail: [junwei@sun.stanford.edu](mailto:junwei@sun.stanford.edu)

## 1. Introduction

Helical features of observed solar magnetic fields have been widely investigated in the previous two decades. Helicity is a physical quantity closely related to the mechanism of solar dynamo, and in this regard, hemispheric preponderance in magnetic (or current) helicity distribution was found and confirmed by different observational groups (Seehafer, 1990; Pevtsov, Canfield, and Metcalf, 1995; Bao and Zhang, 1998; Hagino and Sakurai, 2004; Zhang *et al.*, 2010). On the other hand, the helicity of the magnetic field is supposedly connected with the storage and transfer of energy inside active regions. Pevtsov, Canfield, and Metcalf (1995) and Bao, Ai, and Zhang (2001) found that active regions that did not follow the hemispheric sign rule of helicity tend to be more active than the others in the flare productivity, but this characteristic was not supported by the case study performed by Sakurai and Hagino (2003).

It was found that significant helicity accumulation occurred preceding some major flares (Park *et al.*, 2008). During flares, active regions release magnetic free energy accumulated when magnetic non-potentiality increases. A related flare triggering mechanism is the rapid change of magnetic helicity or annihilation of magnetic helicity (Moon *et al.*, 2002; Kusano *et al.*, 2004).

Another flare triggering mechanism may be related to the plasma motion in solar active regions. As the statistical studies indicate, kinetic helicity is an important parameter that may cause instability and thus magnetic reconnection. The horizontal components of subsurface flows obtained from the ring-diagram analysis, which is a local helioseismology technique, have been used by many authors to investigate the connections between subsurface dynamics and solar eruptive events. An analysis of AR 10486 showed systematic variations in synoptic and daily maps of kinetic helicity that might be the subsurface signatures of the flare events that would occur in this active region later (Komm *et al.*, 2004). A relation was found between the maximum values of the unsigned kinetic helicity density, which was calculated from the subsurface flows associated with each active region, and the total flare X-ray intensity of the active regions (Komm *et al.*, 2005). Mason *et al.* (2006) reported that the maximum unsigned zonal and meridional vorticity components of active regions were correlated with the total flare intensity. More recently, Reinard *et al.* (2010) developed a new parameter, normalized helicity gradient variance, to investigate the connections of subsurface dynamics with solar flares, and found that this parameter was expected to increase two to three days in advance of flare occurrences.

Now, the *Helioseismic and Magnetic Imager* (Scherrer *et al.*, 2012; Schou *et al.*, 2012) onboard the NASA mission *Solar Dynamics Observatory* (SDO/HMI) provides continuous observations of the Sun, and time–distance data-analysis pipeline provides continuous subsurface flow fields for different depths using the HMI data (Zhao *et al.*, 2012). The subsurface flow maps inside active regions give an unprecedented opportunity to study connections between the subsurface dynamics and solar flares with a better spatial resolution and a better temporal cadence. Recently, employing these newly available data, Gao, Zhao, and Zhang (2012) studied the relationship between photospheric current helicity and subsurface kinetic helicity in active regions, and found a quite high correlation between the temporal evolutions of these two different quantities. However, that study did not address whether there was a connection between subsurface properties and occurrences of solar flares. In this paper, we focus on this topic and investigate whether there is such a connection by analyzing a few selected flare-productive active regions. We introduce data acquisition and definition of parameters in Section 2, present our results in Section 3, discuss our results and conclude in Section 4.

**Table 1** Detailed information of flares that are analyzed in this study.

Flare	Date	Start time	Peak time	Disk location	Active region No.
M6.6	2011.02.13	17:28 UT	17:38 UT	S20°, E04°	AR 11158
X2.2	2011.02.15	01:44 UT	01:55 UT	S21°, W21°	AR 11158
X1.5	2011.03.09	23:13 UT	23:23 UT	N08°, W09°	AR 11166
M6.0	2011.08.03	13:17 UT	13:48 UT	N16°, W30°	AR 11261
M9.3	2011.08.04	03:41 UT	03:57 UT	N19°, W36°	AR 11261
M5.3	2011.09.06	01:35 UT	01:50 UT	N14°, W07°	AR 11283
X2.1	2011.09.06	22:12 UT	22:20 UT	N14°, W18°	AR 11283
X1.8	2011.09.07	22:32 UT	22:38 UT	N14°, W28°	AR 11283
M6.7	2011.09.08	15:37 UT	15:46 UT	N14°, W40°	AR 11283
X1.9	2011.09.24	09:21 UT	09:40 UT	N12°, E60°	AR 11302
M7.4	2011.09.25	04:31 UT	04:50 UT	N11°, E47°	AR 11302

## 2. Data Acquisition and Parameters

### 2.1. Data Acquisition

The line-of-sight magnetic field maps used in our analysis are from HMI (Schou *et al.*, 2012), and the subsurface velocity maps are from the HMI time–distance data-analysis pipeline (Zhao *et al.*, 2012). The subsurface velocity maps are typically derived from an 8-hr period, and cover an area of roughly 30° × 30° with active regions located near the center of the area, with a depth coverage from near the surface to about 20 Mm. The spatial resolution of these subsurface velocity maps is 0.06° pixel<sup>-1</sup>. While each flow map is obtained from an 8-hr period, the temporal step used in our analysis is 4 hours. Therefore, each flow map is not completely independent from the maps before and after it, as there is data overlapping between them. X-ray flux density used in this analysis is from GOES (*Geostationary Operational Environment Satellite*) X-ray data lists provided by Space Weather Prediction Center.

For this study, we select five active regions, which produced a total of 11 flares with peak X-ray flux intensity higher than M5.0. The detailed information as regards these flares and active regions is listed in Table 1. One randomly selected sample image showing the magnetic field, overplotted by the subsurface horizontal flow field, is shown for each of five active regions in Figure 1.

### 2.2. Definition of Parameters

Kinetic helicity is defined as

$$H_k = \mathbf{v} \cdot (\nabla \times \mathbf{v}), \tag{1}$$

where  $\mathbf{v}$  is three-dimensional velocity field with three components. Sometimes it is useful to study weighted kinetic helicity, defined as kinetic helicity dividing the square of local speed:

$$\alpha^k = \mathbf{v} \cdot (\nabla \times \mathbf{v}) / |\mathbf{v}|^2. \tag{2}$$

In this study, we only investigate the vertical component of  $\alpha^k$ , and that is

$$\alpha_z^k = v_z (\partial v_x / \partial y - \partial v_y / \partial x) / (v_x^2 + v_y^2 + v_z^2). \tag{3}$$

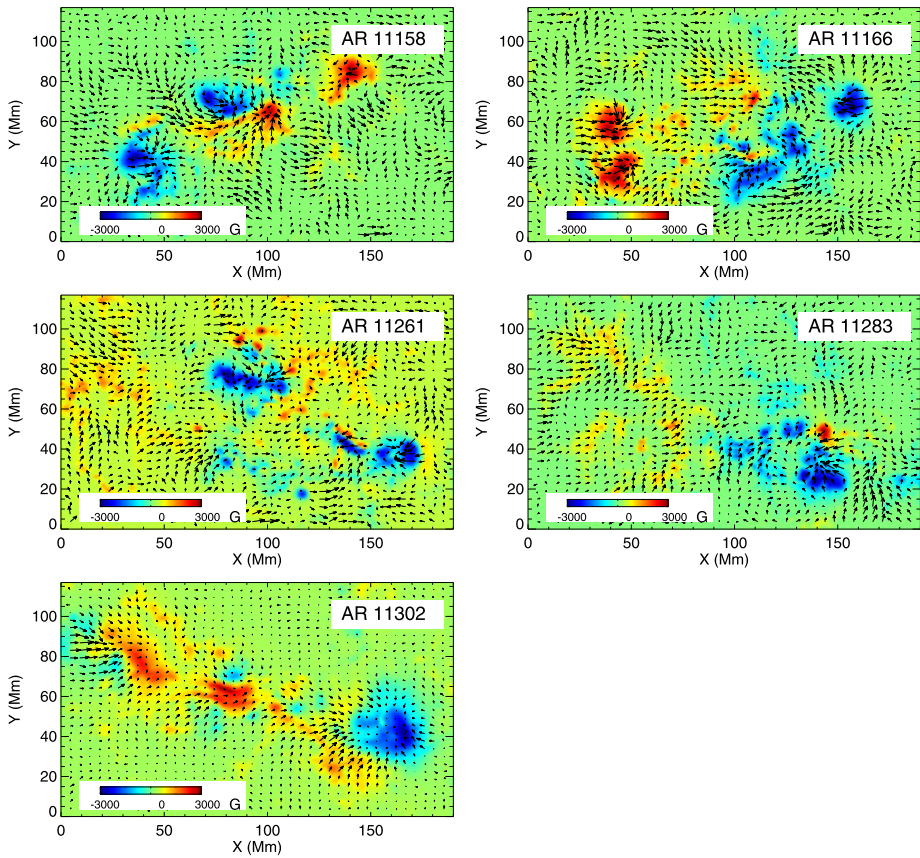


**Figure 1** A randomly selected sample of magnetic field (background image), overplotted by horizontal subsurface flow field (arrows) at the depth of 0–1 Mm, for each of the five studied active regions. The longest arrow in each panel represents the strongest horizontal flow speed: 327 m s<sup>-1</sup>, 381 m s<sup>-1</sup>, 381 m s<sup>-1</sup>, 326 m s<sup>-1</sup>, and 624 m s<sup>-1</sup>, respectively.

When analyzing this parameter, we only use the velocities at the depth of 0–1 Mm. It was already demonstrated that the flow field at this depth was similar to the photospheric flow field derived from combining the correlation tracking and minimization of magnetic induction equations (Liu, Zhao, and Schuck, 2012).

Another parameter we investigate in this study is similar to the Normalized Helicity Gradient Variance (NHGV) defined by Reinard *et al.* (2010). This parameter is obtained by following these steps: differences in helicity at each depth from one time period and the period next to it are first computed:

$$\Delta H_z(t) = H_z(t) - H_z(t - 1), \tag{4}$$

where  $z$  represents the depths of 0–1, 1–3, 3–5, 5–7, 7–9, and 9–11 Mm, respectively, as listed in Zhao *et al.* (2012). Then the spread of the temporal helicity change with depth is determined by summing the changes in  $\Delta H_z$  with depths:

$$\Delta H(t) = \sum_z (\Delta H_z(t) - \Delta H_{z+1}(t)), \tag{5}$$

where  $z$  takes only the first, third, and fifth values. The change in helicity with depth is summed as

$$H(t) = \sum_z (H_z(t) - H_{z+1}(t)), \quad (6)$$

which is expected to capture the overall spread of helicity values. Finally, NHGV is defined as a multiplication of  $\Delta H(t)$  and  $H(t)$ , *i.e.*,

$$\text{NHGV} = \Delta H(t)H(t). \quad (7)$$

Slightly different from the approach taken by Reinard *et al.* (2010), we compute this parameter only in the regions where  $|B_z| > 50$  G and normalize it by the average values in the regions where  $|B_z| < 50$  G. The selection of this criterion threshold, 50 G, is arbitrary, but it is a common practice in similar studies, *e.g.*, Bao and Zhang (1998). When computing both parameters defined above,  $\langle \alpha_z^k \rangle$  and NHGV, we used a Cartesian coordinate system. Since the computation is only limited to active regions and their surrounding areas, there is no significant difference between the Cartesian and spherical coordinates for such computations based on our past experience.

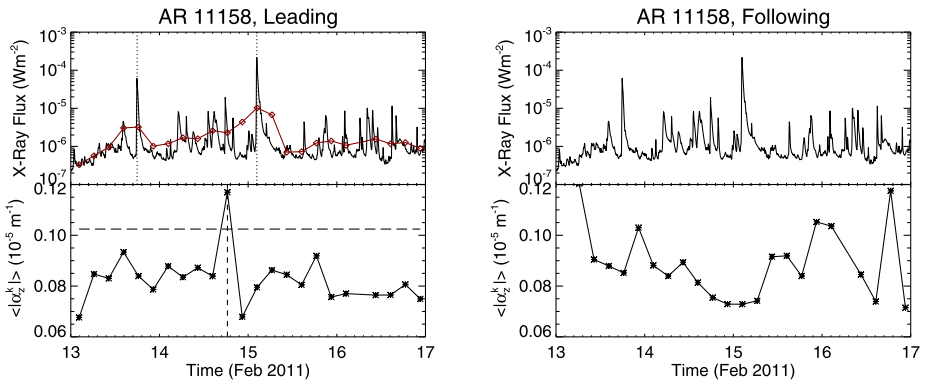
### 3. Results

#### 3.1. Temporal Variation of $\alpha_z^k$ and X-Ray Flux Intensity

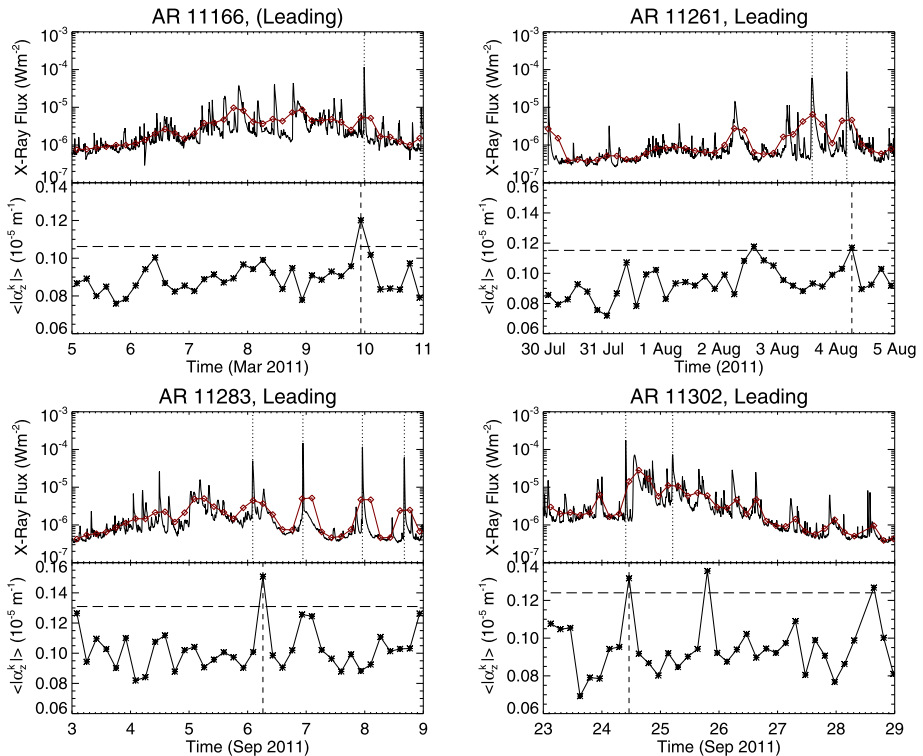
We compute the density of the  $z$ -component of the subsurface kinetic helicity  $\langle \alpha_z^k \rangle$  averaged from areas where  $|B_z| > 50$  G. We also compute the  $\langle \alpha_z^k \rangle$  for each magnetic-field polarity separately by averaging areas where  $B_z > 50$  G and  $B_z < -50$  G (note that depending on the hemispheric location of the active regions, the leading polarity of the active region can be positive or negative). In particular, when we compute  $\langle \alpha_z^k \rangle$ , we only select areas that show prominent kinetic helicity, *i.e.*, where  $|\alpha_z^k| > \langle |\alpha_z^k| \rangle + 1\sigma$ .

Figure 2 shows an example of evolutionary curves of the X-ray flux intensity and the subsurface kinetic helicities calculated for both the leading and the following polarities of NOAA AR 11158. The curves of  $\langle \alpha_z^k \rangle$  show some strong variations, and we define where the  $\langle \alpha_z^k \rangle$  amplitude is  $2\sigma$  above the mean value as an amplitude bump. It can be found there is a bump in  $\langle \alpha_z^k \rangle$  in the leading polarity about seven hours before the start of the X2.2 flare. While the  $\langle \alpha_z^k \rangle$  in the following polarity also shows some amplitude bumps, the connection of these bumps with the powerful X-class flare is not obvious.

Figure 3 shows the evolutionary curves of X-ray flux taken around the flare events that occurred in the other four active regions, together with the evolutionary curves of subsurface kinetic helicity  $\langle \alpha_z^k \rangle$  computed from the leading polarities of these active regions. Since our analyses show that the subsurface  $\langle \alpha_z^k \rangle$  in the following polarities does not exhibit clear connection with the flare occurrences, we do not display results from the following polarities of these active regions. In these four active regions there are a few amplitude bumps in  $\langle \alpha_z^k \rangle$ , and some of them are close in time with the powerful flares. Combining the results shown in Figures 2 and 3, we summarize as follows: among the eight  $\langle \alpha_z^k \rangle$  amplitude bumps, five of them (62.5 %) happened within eight hours, either before or after, of a flare stronger than M5.0; among the 11 flares we studied, five of them (45.5 %) occurred no more than eight hours apart, again either before or after, from an  $\langle \alpha_z^k \rangle$  amplitude bump. Note that eight hours is the time duration of the data used to compute the time–distance subsurface flow maps. There is no clear one-to-one correspondence between the helicity bump and the occurrence



**Figure 2** Evolution of the X-ray flux intensity and the subsurface kinetic helicity for the leading polarity (left panel) and the following polarity (right panel) of NOAA AR 11158. The leading polarity is positive for this active region. The X-ray flux intensity is averaged every eight hours with a four-hour step (shown as red curve in the left panel) so as to better match in temporal periods the data points of the subsurface kinetic helicity. The horizontal dashed line in the left lower panel indicates  $2\sigma$  above the mean, and values above this dashed line are considered as a kinetic helicity bump.



**Figure 3** Same as the left panel of Figure 2, but for the leading polarities in the other four active regions.

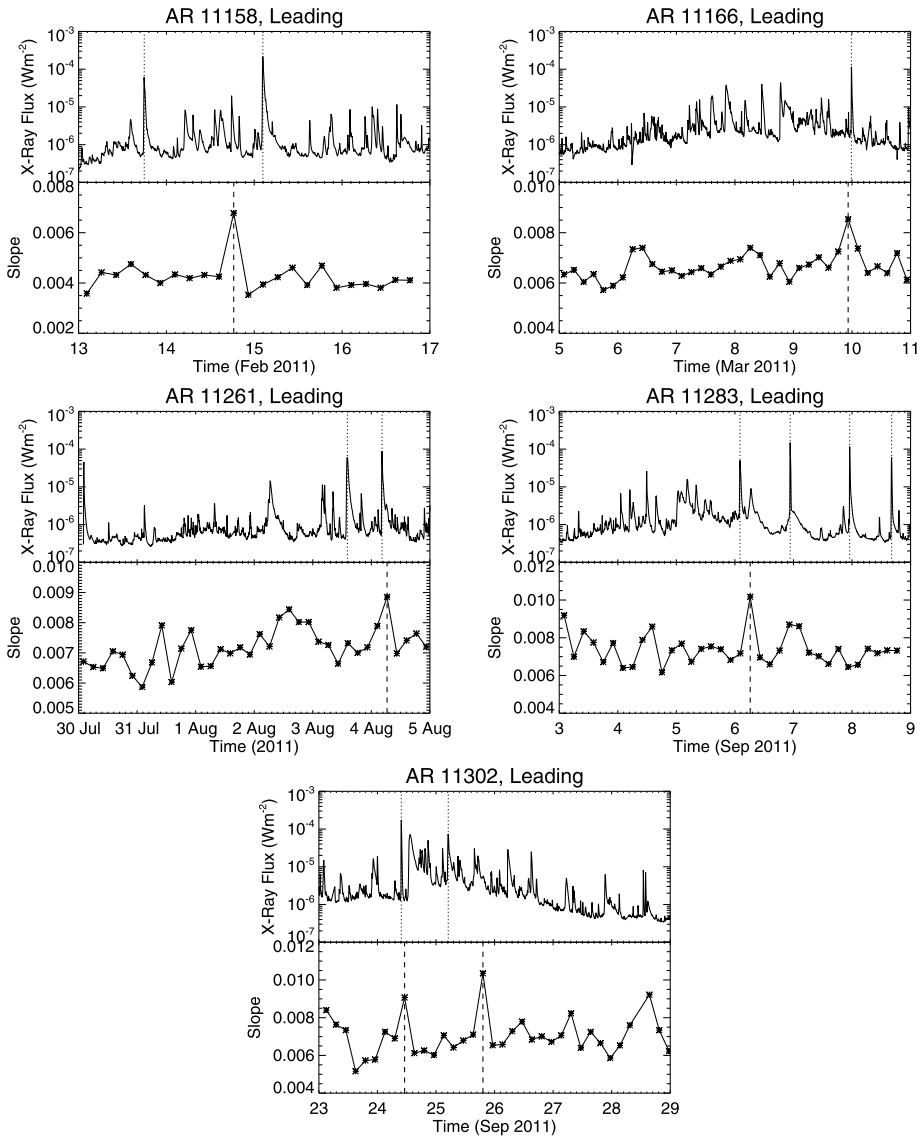


**Figure 4** Evolutionary curves of X-ray flux intensity and the fitted slopes of the subsurface kinetic helicity distribution for all the five active regions.

of a flare. The averaged X-ray flux intensity, shown as red curves in Figures 2 and 3, seems to show a better correlation with the  $\langle \alpha_z^k \rangle$  variations, but the statistical significance is not high.

Furthermore, we establish that the bumps of the subsurface  $\langle \alpha_z^k \rangle$  are a true variation in the profile of kinetic helicity rather than a random enhancement caused by some singular points. For each map of the  $\alpha_z^k$  obtained from one certain time period, we divide all the values of kinetic helicity into ten equal segments covering the minimum value to the maximum. Since each map of  $\alpha_z^k$  may have different minimum and maximum values, these ten segments

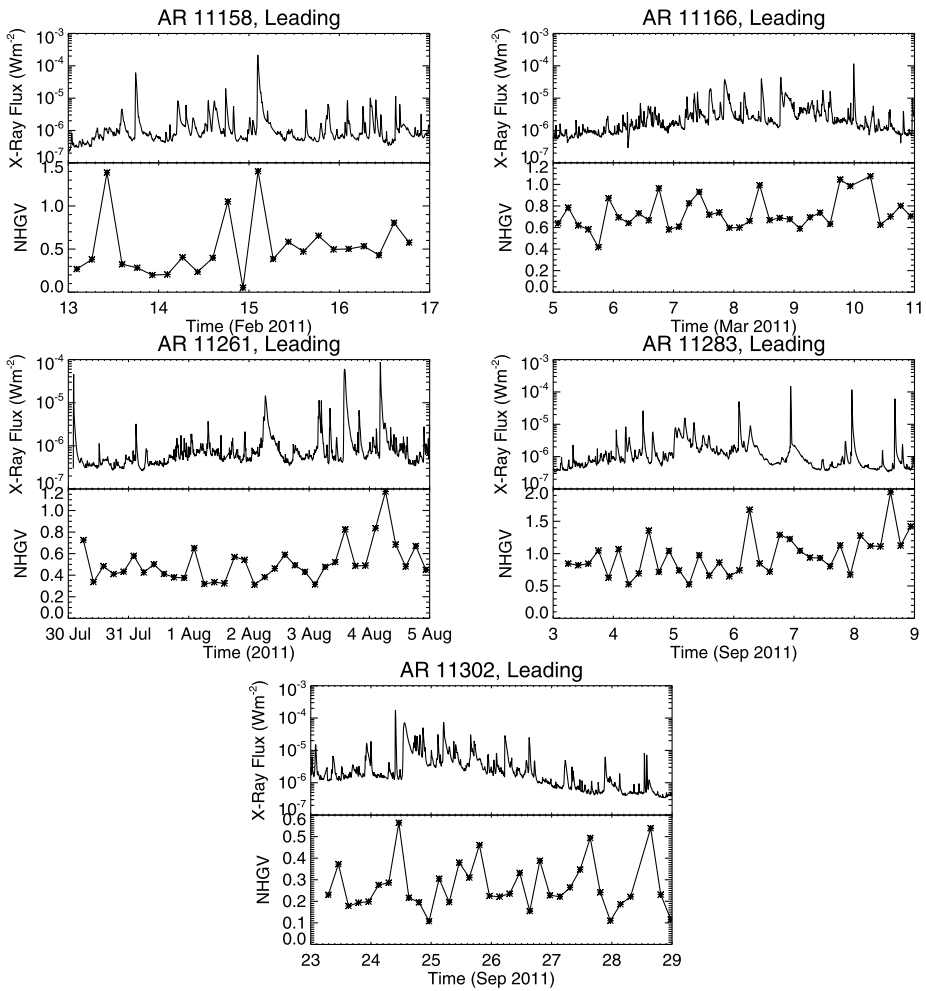


**Figure 5** Evolutionary curves of the X-ray flux intensity and NHGV for all the five active regions. For AR 11158, leading polarity is positive, and for all other four active regions, leading polarity is negative.

may be slightly different for different regions and different time periods. All the data points falling into one segment are averaged to get one mean value. Then the 10 mean values from the ten segments are linearly fitted by adopting orders of segments as arguments to derive a slope, which is believed to reflect the distribution profile of the kinetic helicity. Figure 4 shows all the fitted slopes for the different time periods of different active regions. Comparing the evolutionary curves of these fitted slopes with the variations in  $\langle \alpha_z^k \rangle$  shown in Figures 2 and 3, one is able to find the amplitude bumps seen in Figure 4 match nicely with those seen in Figures 2 and 3. The purpose of this is just to demonstrate that the bumps in the subsurface  $\langle \alpha_z^k \rangle$  seen in Figures 2 and 3 are reliable signals.

### 3.2. Temporal Variation of NHGV and X-Ray Flux Intensity

We perform a similar analysis over the variations of NHGV together with the X-ray flux intensity, and the results over all the five active regions are shown in Figure 5. Once again,



NHGV is only shown for the leading polarity, as there is no clear correspondence between the two quantities in the following polarity. Similar to what is found in Section 3.1, for roughly half of the major flares listed in Table 1, an amplitude bump in NHGV can be found within eight hours of the flare occurrence, either before or after. It is also true that near about half of the large NHGV bumps, powerful flare events occurred. At the moment, we adopt this parameter for a preliminary co-investigation for the result obtained for the  $\langle \alpha_z^k \rangle$ . Quantitative diagnosis of the connection between these two parameters needs further study.

#### 4. Discussion

By analyzing subsurface velocity fields of some flare-productive active regions, together with the X-ray flux intensity, we have found that in about half of the cases the subsurface kinetic helicity shows bumps within eight hours either before or after the flare onset. These bumps in subsurface kinetic helicity are reliable, as can be demonstrated by an alternative approach of analyzing the slopes of distributions of the subsurface kinetic helicity. Meanwhile, our analysis of NHGV, a parameter that reflects kinetic helicity spread in different depth layers of active regions, also shows that major flares are often associated with strong variations in NHGV.

Despite that the  $\langle \alpha_z^k \rangle$  are displayed with a four-hour cadence in Figures 2 and 4, the actual temporal resolution of these data is eight hours, quite poor compared to the rapid development of flare events. Therefore, the bumps found in both  $\langle \alpha_z^k \rangle$  and NHGV within 8-hrs range of flare occurrence may be considered as occurring at about the same time as the flares. It is not very clear to us whether the strong changes in subsurface kinetic helicity and NHGV lead to or help the flare occurrence, or whether these changes in subsurface properties are caused by the occurrences of powerful flares high above the photosphere. However, considering the high mass density and the low plasma  $\beta$  of the subsurface interior, we tend to believe the former rather than the latter.

Previous studies using the subsurface velocity field, derived from the ring-diagram analysis, have found promising connections between subsurface dynamics and flare events (*e.g.* Komm *et al.*, 2005; Mason *et al.*, 2006; Reinard *et al.*, 2010). Both the spatial resolution and the temporal cadence of the velocity fields in these ring-diagram analyses were poorer than the time–distance velocity fields that are used in this study. Although our analysis reveals some promising connections between the subsurface dynamical properties and the flare events, it also shows some ambiguity between them. A clear subsurface indicator of an upcoming major flare may not be there, and most likely, such a subsurface indicator, if there is one, only exists statistically. This prompts us to perform a statistical study once observations of more flare events in more active regions become available from HMI observations. On the other hand, regardless of whether the subsurface properties can be used as flare precursors, the subsurface anomalies that occur close to the flare onset are interesting phenomena, worth further investigation.

**Acknowledgements** SDO is a NASA mission, and HMI project is supported by NASA contract NAS5-02139 to Stanford University. This work is partially supported by the National Natural Science Foundation of China under the grants 11028307, 10921303, 11103037, 11173033, 11221063 and 41174153, and by Chinese Academy of Sciences under grant KJCX2-EW-T07. We thank the anonymous referee for his/her comments and suggestions that helped to improve the quality of this paper.

## References

- Bao, S., Zhang, H.: 1998, *Astrophys. J.* **496**, L43.
- Bao, S., Ai, G., Zhang, H.: 2001, In: Brekke, P., Fleck, B., Gurman, J.B. (eds.) *Recent Insights into the Physics of the Sun and Heliosphere—Highlights from SOHO and Other Space Mission, IAU Symp.* **203**, Astron. Soc. Pac., 247.
- Gao, Y., Zhao, J., Zhang, H.: 2012, *Astrophys. J. Lett.* **761**, L9.
- Hagino, M., Sakurai, T.: 2004, *Publ. Astron. Soc. Pac.* **56**, 831.
- Komm, R.W., Howe, R., González Hernández, I., Hill, F., Haber, D., Hindman, B., Corbard, T.: 2004, In: Danesy, D. (ed.) *SOHO 14 Helio- and Asteroseismology: Towards a Golden Future, ESA SP-559*, ESA, Noordwijk, 520.
- Komm, R., Howe, R., Hill, F., González Hernández, I., Toner, C.: 2005, *Astrophys. J.* **630**, 1184.
- Kusano, K., Maeshiro, T., Yokoyama, T., Sakurai, T.: 2004, *Astrophys. J.* **610**, 537.
- Liu, Y., Zhao, J., Schuck, P.W.: 2012, *Solar Phys.* doi:[10.1007/s11207-012-0089-3](https://doi.org/10.1007/s11207-012-0089-3).
- Mason, D., Komm, R., Hill, F., Howe, R., Haber, D., Hindman, B.: 2006, *Astrophys. J.* **645**, 1543.
- Moon, Y.J., Chae, J., Choe, G.S., Wang, H.M., Park, Y.D., Yun, H.S., Yurchyshyn, V., Goode, P.R.: 2002, *Astrophys. J.* **574**, 1066.
- Park, S., Lee, J., Choe, G.S., Chae, J., Jeong, H., Yang, G., Jing, J., Wang, H.: 2008, *Astrophys. J.* **686**, 1397.
- Pevtsov, A.A., Canfield, R.C., Metcalf, T.R.: 1995, *Astrophys. J.* **440**, 109.
- Reinard, A.A., Henthorn, J., Komm, R., Hill, F.: 2010, *Astrophys. J. Lett.* **710**, L121.
- Sakurai, T., Hagino, M.: 2003, *Adv. Space Res.* **32**, 1943.
- Scherrer, P.H., Schou, J., Bush, R.I., Kosovichev, A.G., Bogart, R.S., Hoeksema, J.T., Liu, Y., Duvall, T.L., Jr., Zhao, J., Title, A.M., et al.: 2012, *Solar Phys.* **275**, 207.
- Schou, J., Scherrer, P.H., Bush, R.I., Wachter, R., Couvidat, S., Rabello-Soares, M.C., Bogart, R.S., Hoeksema, J.T., Liu, Y., Duvall, T.L., Jr., et al.: 2012, *Solar Phys.* **275**, 229.
- Seehafer, N.: 1990, *Solar Phys.* **125**, 219.
- Zhang, H., Sakurai, T., Pevtsov, A., Gao, Y., Xu, H., Sokoloff, D., Kuzanyan, K.: 2010, *Mon. Not. Roy. Astron. Soc.* **402**, L30.
- Zhao, J., Couvidat, S., Bogart, R.S., Parchevsky, K.V., Birch, A.C., Duvall, T.L. Jr., Beck, J.G., Kosovichev, A.G., Scherrer, P.H.: 2012, *Solar Phys.* **275**, 375.